

University of Massachusetts Amherst
ScholarWorks@UMass Amherst

Mathematics and Statistics Department Faculty
Publication Series

Mathematics and Statistics

2015

Dark Solitons Near Potential and Nonlinearity Steps

F. Tsitoura

University of Athens

Z. A. Anastassi

Qatar University

J. L. Marzuola

University of North Carolina

P. G. Kevrekidis

University of Massachusetts, Amherst

D. J. Frantzeskakis

University of Athens

Follow this and additional works at: https://scholarworks.umass.edu/math_faculty_pubs

Recommended Citation

Tsitoura, F.; Anastassi, Z. A.; Marzuola, J. L.; Kevrekidis, P. G.; and Frantzeskakis, D. J., "Dark Solitons Near Potential and Nonlinearity Steps" (2015). *Mathematics and Statistics Department Faculty Publication Series*. 1238.

Retrieved from https://scholarworks.umass.edu/math_faculty_pubs/1238

This Article is brought to you for free and open access by the Mathematics and Statistics at ScholarWorks@UMass Amherst. It has been accepted for inclusion in Mathematics and Statistics Department Faculty Publication Series by an authorized administrator of ScholarWorks@UMass Amherst. For more information, please contact scholarworks@library.umass.edu.

Dark solitons near potential and nonlinearity steps

F. Tsitoura,¹ Z. A. Anastassi,² J. L. Marzuola,³ P. G. Kevrekidis,^{4,5} and D. J. Frantzeskakis¹

¹*Department of Physics, University of Athens, Panepistimiopolis, Zografos, Athens 15784, Greece*

²*Department of Mathematics, Statistics and Physics, College of Arts and Sciences, Qatar University, 2713 Doha, Qatar*

³*Department of Mathematics, University of North Carolina, Chapel Hill, NC 27599, USA*

⁴*Department of Mathematics and Statistics, University of Massachusetts, Amherst, Massachusetts 01003-4515 USA*

⁵*Center for Nonlinear Studies and Theoretical Division,
Los Alamos National Laboratory, Los Alamos, NM 87544*

We study dark solitons near potential and nonlinearity steps and combinations thereof, forming rectangular barriers. This setting is relevant to the contexts of atomic Bose-Einstein condensates (where such steps can be realized by using proper external fields) and nonlinear optics (for beam propagation near interfaces separating optical media of different refractive indices). We use perturbation theory to develop an equivalent particle theory, describing the matter-wave or optical soliton dynamics as the motion of a particle in an effective potential. This Newtonian dynamical problem provides information for the soliton statics and dynamics, including scenarios of reflection, transmission, or quasi-trapping at such steps. The case of multiple such steps and its connection to barrier potentials is also touched upon. Our analytical predictions are found to be in very good agreement with the corresponding numerical results.

PACS numbers: 03.75.Lm, 05.45.Yv

I. INTRODUCTION

The interaction of solitons with impurities is a fundamental problem that has been considered in various branches of physics – predominantly in nonlinear wave theory [1] and solid state physics [2] – as well as in applied mathematics (see, e.g., recent work [3] and references therein). Especially, in the framework of the nonlinear Schrödinger (NLS) equation, the interaction of bright and dark solitons with δ -like impurities has been investigated in many works (see, e.g., Refs. [4–8]). Relevant studies in the physics of atomic Bose-Einstein condensates (BECs) have also been performed (see, e.g., Refs. [9–13]), as well as in settings involving potential wells [14, 15] and barriers [16, 17] (see also Ref. [18] for earlier work in a similar model). In this context, localized impurities can be created as focused far-detuned laser beams, and have already been used in experiments involving dark solitons [19, 20]. Furthermore, experimental results on the scattering of matter-wave bright solitons on Gaussian barriers in either ^7Li [21] or ^{85}Rb [22] BECs have been reported as well. More recently, such soliton-defect interactions were also explored in the case of multi-component BECs and dark-bright solitons, both in theory [23] and in an experiment [24].

On the other hand, much attention has been paid to BECs with spatially modulated interatomic interactions, so-called “collisionally inhomogeneous condensates” [25, 26]; for a review with a particular bend towards periodic such interactions see also Ref. [27]). Relevant studies in this context have explored a variety of interesting phenomena: these include, but are not limited to adiabatic compression of matter-waves [25, 28], Bloch oscillations of solitons [25], emission of atomic solitons [29, 30], scattering of matter waves through barriers [31], emergence of instabilities of solitary waves due to periodic variations in the scattering length [32], formation of stable condensates exhibiting both attractive and repulsive interatomic interactions [33], solitons in combined linear and nonlinear potentials [34–38], generation of solitons [39] and

vortex rings [40], control of Faraday waves [41], vortex dipole dynamics in spinor BECs [42], and others.

Here, we consider a combination of the above settings, namely we consider a one-dimensional (1D) setting involving potential and nonlinearity steps, as well as pertinent rectangular barriers, and study statics, dynamics and scattering of dark solitons. In the BEC context, recent experiments have demonstrated robust dark solitons in the quasi-1D setting [43]. In addition, potential steps in BECs can be realized by trapping potentials featuring piece-wise constant profiles (see, e.g., Refs. [44, 45] and discussion in the next Section). Furthermore, nonlinearity steps can be realized too, upon employing magnetically [46] or optically [47] induced Feshbach resonances, that can be used to properly tune the interatomic interactions strength – see, e.g., more details in Refs. [30, 35] and discussion in the next Section.

Such a setting involving potential and nonlinearity steps, finds also applications in the context of nonlinear optics. There, effectively infinitely long potential and nonlinearity steps of constant and finite height, describe interfaces separating optical media characterized by different linear and nonlinear refractive indices [48]. In such settings, it has been shown [49–52] that the dynamics of self-focused light channels – in the form of spatial bright solitons – can be effectively described by the motion of an equivalent particle in effective step-like potentials. This “equivalent particle theory” actually corresponds to the adiabatic approximation of the perturbation theory of solitons [1], while reflection-induced radiation effects can be described at a higher-order approximation [50, 51]. Note that similar studies, but for dark solitons in settings involving potential steps and rectangular barriers, have also been performed – see, e.g., Ref. [53] for an effective particle theory, and Refs. [54–56] for numerical studies of reflection-induced radiation effects. However, to the best of our knowledge, the statics and dynamics of dark solitons near potential and nonlinearity steps, have not been systematically considered so far in the literature, although a special

version of such a setting has been touch upon in Ref. [35].

It is our purpose, in this work, to address this problem. In particular, our investigation and a description of our presentation is as follows. First, in Sec. II, we provide the description and modeling of the problem; although this is done in the context of atomic BECs, our model can straightforwardly be used for similar considerations in the context of optics, as mentioned above. In the same Section, we apply perturbation theory for dark solitons to show that, in the adiabatic approximation, soliton dynamics is described by the motion of an equivalent particle in an effective potential. The latter has a tanh-profile, but – in the presence of the nonlinearity step – can also exhibit an elliptic and a hyperbolic fixed point. We show that stationary soliton states do exist at the fixed points of the effective potential, but are unstable (albeit in different ways, as is explained below) according to a Bogoliubov-de Gennes (BdG) analysis [57, 58] that we perform; we also use an analytical approximation to derive the unstable eigenvalues as functions of the magnitudes of the potential/nonlinearity steps. In Sec. III we study the soliton dynamics for various parameter values, pertaining to different forms of the effective potential, including the case of rectangular barriers formed by combination of adjacent potential and nonlinearity steps. Our numerical results – in both statics and dynamics – are found to be in very good agreement with the analytical predictions. We also investigate the possibility of soliton trapping in the vicinity of the hyperbolic fixed point of the effective potential; note that such states could be characterized as “surface dark solitons”, as they are formed at linear/nonlinear interfaces separating different optical or atomic media. We show that quasi-trapping of solitons is possible, in the case where nonlinearity steps are present; the pertinent (finite) trapping time is found to be of the order of several hundreds of milliseconds, which suggests that such soliton quasi-trapping could be observable in real BEC experiments. Finally, in Sec. IV we summarize our findings, discuss our conclusions, and provide perspectives for future studies.

II. MODEL AND ANALYTICAL CONSIDERATIONS

A. Setup

As noted in the Introduction, our formulation originates from the context of atomic BECs in the mean-field picture [57]. We thus consider a quasi-1D setting whereby matter waves, described by the macroscopic wave function $\Psi(x, t)$, are oriented along the x -direction and are confined in a strongly anisotropic (quasi-1D) trap. The latter, has the form of a rectangular box of lengths $L_x \gg L_y = L_z \equiv L_\perp$, with the transverse length L_\perp being on the order of the healing length ξ . Such a box-like trapping potential, $V_b(x)$, can be approximated by a super-Gaussian function, of the form:

$$V_b(x) = V_0 \left[1 - \exp \left(- \left(\frac{x}{w} \right)^\gamma \right) \right], \quad (1)$$

where V_0 and w denote the trap amplitude and width, respectively. The particular value of the exponent $\gamma \gg 1$ is not

especially important; here we use $\gamma = 50$. In this setting, our aim is to consider dark solitons near potential and nonlinearity steps, located at $x = L$. To model such a situation, we start from the Gross-Pitaevskii (GP) equation [57, 58]:

$$i\hbar \frac{\partial \Psi}{\partial t} = \left[- \frac{\hbar^2}{2m} \partial_x^2 + g(x)|\Psi|^2 + V(x) \right] \Psi, \quad (2)$$

Here, $\Psi(x, t)$ is the mean-field wave function, m is the atomic mass, $V(x)$ represents the external potential, while $g_{1D}(x) = (9/4L_\perp^2)g_{3D}$ is the effectively 1D interaction strength, with $g_{3D} = 4\pi\hbar^2\alpha(x)/m$ being its 3D counterpart and $\alpha(x)$ being the scattering length (assumed to be $\alpha > 0, \forall x$, corresponding to repulsive interatomic interactions). The external potential and the scattering length are then taken to be of the form:

$$V(x) = V_b(x) + \begin{cases} V_L, & x < L \\ V_R, & x > L \end{cases}, \quad (3)$$

$$\alpha(x) = \begin{cases} \alpha_L, & x < L \\ \alpha_R, & x > L \end{cases}, \quad (4)$$

where $V_{L,R}$ and $\alpha_{L,R}$ are constant values of the potential and scattering length, to the left and right of $x = L$, where respective steps take place.

Notice that such potential steps may be realized in present BEC experiments upon employing a detuned laser beam shined over a razor edge to make a sharp barrier, with the diffraction-limited fall-off of the laser intensity being smaller than the healing length of the condensate; in such a situation, the potential can be effectively described by a step function. On the other hand, the implementation of nonlinearity steps can be based on the interaction tunability of specific atomic species by applying external magnetic or optical fields [46, 47]. For instance, confining ultracold atoms in an elongated trapping potential near the surface of an atom chip [59] allows for appropriate local engineering of the scattering length to form steps (of varying widths), where the atom-surface separation sets a scale for achievable minimum step widths. The trapping potential can be formed optically, possibly also by a suitable combination of optical and magnetic fields (see Ref. [35] for a relevant discussion).

Measuring the longitudinal coordinate x in units of $\sqrt{2}\xi$ (where $\xi \equiv \hbar/\sqrt{2mng_{1D}}$ is the healing length), time t in units of $\sqrt{2}\xi/c_s$ (where $c_s \equiv \sqrt{g_{1D}n/m}$ is the speed of sound and n is the peak density), and energy in units of $g_{1D}n$, we cast Eq. (2) to the following dimensionless form (see Ref. [60]):

$$i \frac{\partial u}{\partial t} = - \frac{1}{2} \frac{\partial^2 u}{\partial x^2} + \frac{\alpha(x)}{\alpha_L} |u|^2 u + V(x)u, \quad (5)$$

where $u = \sqrt{n}\Psi$. Unless stated otherwise, in the simulations below we fix the parameter values as follows: $V_0 = 10$ and $w = 250$ (for the box potential), $V_L = 0$ and $V_R = \pm 0.01$ for the potential step, as well as $\alpha_L = 1$ and $\alpha_R \in [0.9, 1.1]$ for the nonlinearity step. Nevertheless, our theoretical approach is general (and will be kept as such in the exposition that follows in this section).

Here we should mention that Eq. (5) can also be applied in the context of nonlinear optics [48]: in this case, u represents

the complex electric field envelope, t is the propagation distance and x is the transverse direction, while $V(x)$ and $\alpha(x)$ describe the (transverse) spatial profile of the linear and nonlinear parts of the refractive index [36]. This way, Eq. (5) can be used for the study of optical beams, carrying dark solitons, near interfaces separating different optical media, with (different) defocusing Kerr nonlinearities.

B. Perturbation theory and equivalent particle picture

Assuming that, to a first approximation, the box potential can be neglected, we consider the dynamics of a dark soliton, which is located in the region $x < L$, and moves to the right, towards the potential and nonlinearity steps (similar considerations for a soliton located in the region $x > L$ and moving to the left are straightforward). In such a case, we seek for a solution of Eq. (5) in the form:

$$u(x, t) = \sqrt{\mu_L - V_L} \exp(-i\mu_L t) v(x, t), \quad (6)$$

where μ_L is the chemical potential, and the $v(x, t)$ is the wavefunction of the dark soliton. Then, introducing the transformations $t \rightarrow (\mu_L - V_L)t$ and $x \rightarrow \sqrt{\mu_L - V_L}x$, we express Eq. (5) as a perturbed NLS equation for the dark soliton:

$$i \frac{\partial v}{\partial t} + \frac{1}{2} \frac{\partial^2 v}{\partial x^2} - (|v|^2 - 1)v = P(v). \quad (7)$$

Here, the functional perturbation $P(v)$ has the form:

$$P(v) = (A + B|v|^2)v\mathcal{H}(x - L), \quad (8)$$

where \mathcal{H} is the Heaviside step function, and coefficients A, B are given by:

$$A = \frac{V_R - V_L}{\mu_L - V_L}, \quad B = \frac{\alpha_R}{\alpha_L} - 1. \quad (9)$$

These coefficients, which set the magnitudes of the potential and nonlinearity steps, are assumed to be small. Such a situation corresponds, e.g., to the case where $\mu_L = 1$, $V_L = 0$, $V_R \sim \epsilon$, and $\alpha_R/\alpha_L \sim 1$, where $0 < \epsilon \ll 1$ is a formal small parameter (this choice will be used in our simulations below). In the present work, we assume that the jump from left to right is ‘‘sharp’’, i.e., we do not explore the additional possibility of a finite width interface. If such a finite width was present but was the same between the linear and nonlinear interface, essentially the formulation below would still be applicable, with the Heaviside function above substituted by a suitable smoothed variant (e.g. a tanh functional form). A more complicated setting deferred for future studies would involve the existence of two separate widths in the linear and nonlinear step and the length scale competition that that could involve.

Equation (7) can be studied analytically upon employing perturbation theory for dark solitons (see, e.g., Refs. [61–63]): first we note that, in the absence of the perturbation (8), Eq. (7) has a dark soliton solution of the form:

$$v(x, t) = \cos \phi \tanh X + i \sin \phi, \quad (10)$$

where $X = \cos \phi [x - x_0(t)]$ is the soliton coordinate, ϕ is the soliton phase angle ($|\phi| < \pi/2$) describing the darkness of the soliton, $\cos \phi$ is the soliton depth ($\phi = 0$ and $\phi \neq 0$ correspond to stationary black solitons and gray solitons, respectively), while $x_0(t)$ and $dx_0/dt = \sin \phi$ denote the soliton center and velocity, respectively. Then, considering an adiabatic evolution of the dark soliton, we assume that in the presence of the perturbation the dark soliton parameters become slowly-varying unknown functions of time t . Thus, the soliton phase angle becomes $\phi \rightarrow \phi(t)$ and, as a result, the soliton coordinate becomes $X = \cos \phi(t)(x - x_0(t))$, with $dx_0(t)/dt = \sin \phi(t)$.

The evolution of the soliton phase angle can be found by means of the evolution of the renormalized soliton energy, E_{ds} , given by [61, 62]:

$$E_{ds} = \frac{1}{2} \int_{-\infty}^{\infty} [|v_x|^2 + (|v|^2 - 1)^2] dx. \quad (11)$$

Employing Eq. (10), it can readily be found that $dE_{ds}/dt = -4 \cos^2 \phi \sin \phi d\phi/dt$. On the other hand, using Eq. (7) and its complex conjugate, yields the evolution of the renormalized soliton energy: $dE_{ds}/dt = - \int_{-\infty}^{+\infty} (P\bar{v}_t + \bar{P}v_t) dx$, where bar denotes complex conjugate. Then, the above expressions for dE_{ds}/dt yield the evolution of ϕ , namely

$$\frac{d\phi}{dt} = \frac{1}{2 \cos^2 \phi \sin \phi} \text{Re} \left\{ \int_{-\infty}^{+\infty} P(v)\bar{v}_t dx \right\}. \quad (12)$$

Inserting the perturbation (8) into Eq. (12), and performing the integration, we obtain the following result:

$$\begin{aligned} \frac{d\phi}{dt} = & - \frac{1}{4} (A + B) \text{sech}^2 (L - x_0) \\ & + \frac{1}{8} B \text{sech}^4 (L - x_0), \end{aligned} \quad (13)$$

where we have considered the case of nearly stationary (black) solitons with $\cos \phi \approx 1$ (and $\sin \phi \approx \phi$). Combining Eq. (13) with the above mentioned equation for the soliton velocity, $dx_0(t)/dt = \sin \phi(t)$, we can readily derive the following equation for motion for the soliton center:

$$\frac{d^2 x_0}{dt^2} = - \frac{dW}{dx_0}, \quad (14)$$

where the effective potential $W(x_0)$ is given by:

$$\begin{aligned} W(x_0) = & - \frac{1}{8} (2A + B) \tanh (L - x_0) \\ & - \frac{1}{24} B \tanh^3 (L - x_0). \end{aligned} \quad (15)$$

C. Forms of the effective potential

The form of the effective potential suggests that fixed points, where – potentially – dark solitons may be trapped, exist only in the presence of the nonlinearity step ($B \neq 0$). I.e., it is the competition between the linear and nonlinear step that

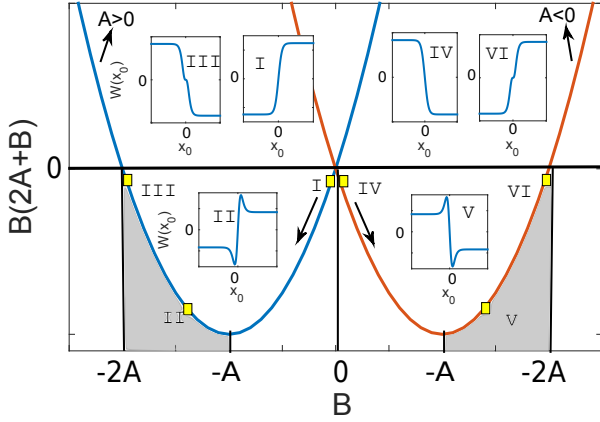


FIG. 1: Sketch showing domains of existence of fixed points of the effective potential $W(x_0)$ (depicted by gray areas) for $A > 0$ (blue line) and $A < 0$ (red line). The insets I–III (IV–VI) show the form of $W(x_0)$, starting from – and ending to – a small finite value of nonlinearity step B , which is gradually decreased (increased) for $A > 0$ ($A < 0$), cf. black arrows. Small rectangular (yellow) points indicate parameter values corresponding to the forms of $W(x_0)$ shown in the insets I – VI.

enable the presence of fixed points and associated more complex dynamics; in the presence of solely a linear step, the dark soliton encounters solely a step potential, similarly to what is the case for its bright sibling [18]; see also below.

In fact, in our setting it is straightforward to find that there exist two fixed points, located at:

$$x_{0\pm} = \frac{1}{2} \ln \left(\frac{-A \mp \sqrt{-B(2A+B)}}{A+B} \right), \quad (16)$$

for $B(2A+B) < 0$ and $-2A < B < -A$, for $A > 0$, or $-A < B < -2A$, for $A < 0$. In Fig. 1 we plot $B(2A+B)$ as a function of B , for $A > 0$ (blue line) and $A < 0$ (red line). The corresponding domains of existence of the fixed points, are also depicted by the gray areas. Insets show typical profiles of the effective potential $W(x_0)$, for different values of B , which we discuss in more detail below. From the figure (as well as from Eq. (16) itself), the saddle-center nature of the bifurcation of the two fixed points, which are generated concurrently “out of the blue sky” is immediately evident.

First, we consider the case of the absence of the nonlinearity step, $B = 0$, as shown in the insets I and IV of Fig. 1, for $A > 0$ and $A < 0$, respectively. In this case, $W(x_0)$ assumes a step profile, induced by the potential step. This form is preserved in the presence of a finite nonlinearity step, $B \neq 0$, namely for $-A < B < 0$ and $0 < B < -A$, in the cases $A > 0$ and $A < 0$, respectively.

A more interesting situation occurs when the nonlinearity step further decreases (increases), and takes values $-2A < B < -A$ for $A > 0$, or $-A < B < -2A$ for $A < 0$. In this case, the effective potential features a local minimum (maximum), i.e., an elliptic (hyperbolic) fixed point, in the region $x < 0$ ($x > 0$) for $A > 0$ emerge (as per the saddle-center

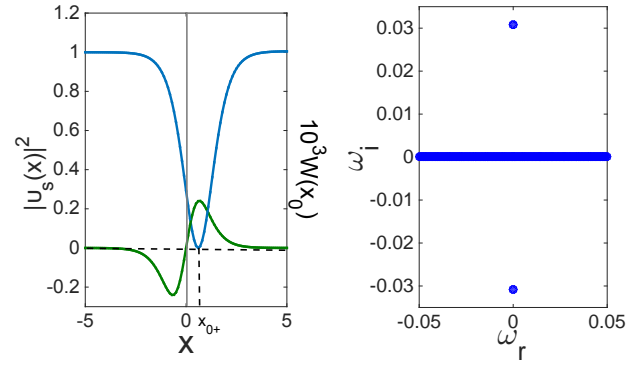


FIG. 2: (Color online) Left panel: density profile of the stationary soliton (blue line) at the hyperbolic fixed point $x_{0+} = 0.66$, as found numerically, using the ansatz $v_s(x) = [1 - V(x)]^{1/2} \tanh(x)$ in Eq. (17), for $\alpha_R/\alpha_L = 0.985$, $V_R = 0.01$, $V_L = 0$, $\mu_L = 1$; green line illustrates the corresponding effective potential $W(x_0)$. Right panel: corresponding spectral plane (ω_r , ω_i) of the corresponding eigenfrequencies, illustrating an exponential growth due to an imaginary eigenfrequency pair.

bifurcation mentioned above) close to the location of the potential and nonlinearity steps, i.e., near $x = 0$; a similar situation occurs for $A < 0$, but the local minimum becoming a local maximum, and vice versa. The locations $x_{0\pm}$ of the fixed points are given by Eq. (16); as an example, using parameter values $V_L = 0$, $V_R = -0.01$, $\alpha_L = 1$ and $\alpha_R = 1.015$, we find that $x_{0+} = 0.66$ ($x_{0-} = -0.66$) for the elliptic (hyperbolic) fixed point.

As the nonlinearity step becomes deeper, the asymptotes (for $x \rightarrow \pm\infty$) of $W(x_0)$ become smaller and eventually vanish. For fixed $V_L = 0$ (and $\mu_L = 1$), Eq. (15) shows that this happens for $B = -(3/2)A$; in this case, the potential features a “spiky” profile, in the vicinity of $x = 0$ (see, e.g., upper panel of Fig. 6 below). For $B < -(3/2)A$, the asymptotes of $W(x_0)$ become finite again, and take a positive (negative) value for $x < 0$, and a negative (positive) value for $x > 0$, in the case $A > 0$ ($A < 0$). The spiky profile of $W(x_0)$ in the vicinity of $x = 0$ is preserved in this case too, but as B decreases it eventually disappears, as shown in the insets III and VI of Fig. 1.

D. Solitons at the fixed points of the effective potential

The above analysis poses an interesting question regarding the existence of stationary solitons of Eq. (5) at the fixed points of the effective potential. To address this question, we use the ansatz $u(x, t) = \exp(-it)v_s(x)$, for a stationary soliton $v_s(x)$, and obtain from Eq. (5) the equation:

$$v_s = -\frac{1}{2} \frac{d^2 v_s}{dx^2} + \frac{\alpha(x)}{\alpha_L} |v_s|^2 v_s + V(x) v_s. \quad (17)$$

Notice that we have assumed without loss of generality a unit frequency solution; the formulation below can be used at will for any other frequency. The above equation is then solved

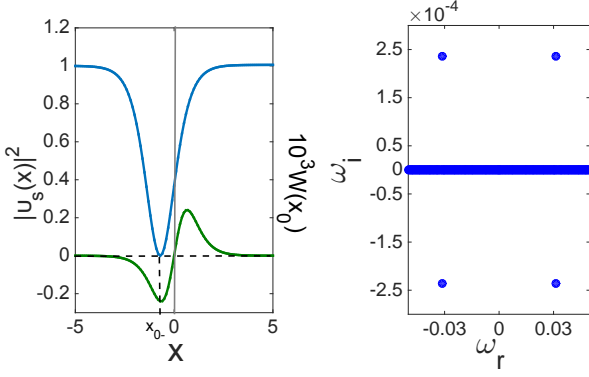


FIG. 3: (Color online) Same as Fig. 2, but for a soliton located at the elliptic fixed point $x_{0-} = -0.66$; this state is found using the initial ansatz $v_s(x) = [1 - V(x)]^{1/2} \tanh(x + 0.2)$. The spectral plane in the right panel illustrates an oscillatory growth due to the presence of a complex quartet of eigenfrequencies.

numerically, by means of Newton's method, employing the ansatz (for $L = 0$):

$$v_s(x) = [1 - V(x)]^{1/2} \tanh(x - x_0). \quad (18)$$

As shown in the left panel of Fig. 2, assuming an ansatz within Eq. (18) in which the soliton is initially placed at $x_0 = 0$, we find a steady state exactly at the hyperbolic fixed point $x_{0+} = 0.66$, as found from Eq. (16). On the other hand, the left panel of Fig. 3 shows a case where the initial guess is assumed in Eq. (18) to have a soliton positioned at $x_0 = -0.2$, which leads to a stationary soliton located exactly at the elliptic fixed point $x_{0-} = -0.66$ predicted by Eq. (16).

It is now relevant to study the stability of these stationary soliton states, performing a Bogoliubov-de Gennes (BdG) analysis [57, 58, 62]. We thus consider small perturbations of $v_s(x)$, and seek solutions of Eq. (17) of the form:

$$u(x, t) = e^{-it} [v_s(x) + \delta (b(x)e^{-i\omega t} + \bar{c}(x)e^{i\bar{\omega}t})], \quad (19)$$

where $(b(x), c(x))$ are eigenmodes, $\omega = \omega_r + i\omega_i$ are (generally complex) eigenfrequencies, and $\delta \ll 1$. Notice that the occurrence of a complex eigenfrequency always leads to a dynamic instability; thus, a linearly stable configuration is tantamount to $\omega_i = 0$ (i.e., all eigenfrequencies are real).

Substituting Eq. (19) into Eq. (5), and linearizing with respect to δ , we derive the following BdG equations:

$$\left[\hat{H} - 1 + 2 \frac{\alpha(x)}{\alpha_L} v_s^2 \right] b + \frac{\alpha(x)}{\alpha_L} v_s^2 c = \omega b, \quad (20)$$

$$\left[\hat{H} - 1 + 2 \frac{\alpha(x)}{\alpha_L} v_s^2 \right] c + \frac{\alpha(x)}{\alpha_L} v_s^2 b = -\omega c, \quad (21)$$

where $\hat{H} = -(1/2)\partial_x^2 + V(x)$ is the single particle operator. This eigenvalue problem is then solved numerically. Examples of the stationary dark solitons at the fixed points $x_{0\pm}$ of the effective potential W , as well as their corresponding BdG spectra, are shown in Figs. 2 and 3. It is observed that the solitons are dynamically unstable, as seen by the presence of

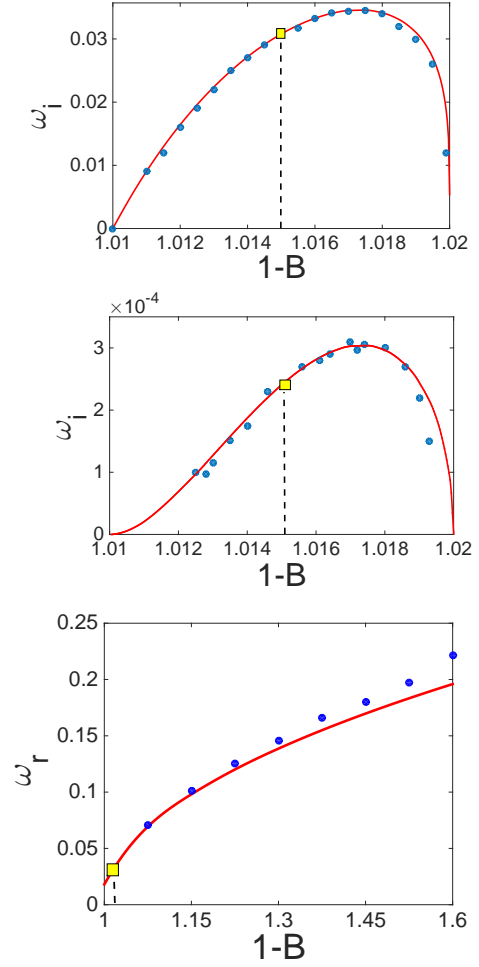


FIG. 4: (Color online) Top panel: the imaginary part of the eigenfrequency, ω_i , as a function of $1 - B$ (with $B < 0$), for a soliton located at the hyperbolic fixed point, $x = x_{0+}$. Middle and bottom panels show the dependence of imaginary and real parts, ω_i and ω_r , of the eigenfrequency on $1 - B$, for a soliton located at the elliptic fixed point, $x = x_{0-}$, i.e., the case that leads to an eigenfrequency quartet. Solid blue curves correspond to the analytical prediction [cf. Eqs. (23) and (24)], blue circles depict numerical results, while yellow squares depict eigenfrequency values corresponding to the cases shown in Figs. 2 and 3. For the top and middle panels $A = 0.01$, while for the bottom panel $A = -(2/3)B$; in all cases, $\mu_L = 1$.

eigenfrequencies with nonzero imaginary part in the spectra, although the mechanisms of instability are distinctly different between the two cases (of Figs. 2 and 3).

To better understand these instabilities, and also provide an analytical estimate for the relevant eigenfrequencies, we may follow the analysis of Ref. [64]; see also Ref. [65] for application of this theory to the case of a periodic, piecewise-constant scattering length setting. According to these works, solitons persist in the presence of the perturbation $P(v)$ of Eq. (8) (of strength A , $B \sim \epsilon$) provided that the Melnikov function con-

dition

$$M'(x_0) = \int_{-\infty}^{+\infty} \frac{\partial P(v)}{\partial x} \operatorname{sech}^2(x - x_0) dx = 0, \quad (22)$$

possesses at least one root, say \tilde{x}_0 . Then, the stability of the dark soliton solutions at $x_{0\pm}$ depends on the sign of the derivative of the function in Eq. (22), evaluated at \tilde{x}_0 : an instability occurs, with one imaginary eigenfrequency pair for $\epsilon M''(\tilde{x}_0) < 0$, and with exactly one complex eigenfrequency quartet for $\epsilon M''(\tilde{x}_0) > 0$. The instability is dictated by the translational eigenvalue, which bifurcates from the origin as soon as the perturbation is present. For $\epsilon M''(\tilde{x}_0) < 0$, the relevant eigenfrequency pair moves along the imaginary axis, leading to an immediate instability associated with exponential growth of a perturbation along the relevant eigendirection. On the other hand, for $\epsilon M''(\tilde{x}_0) > 0$, the eigenfrequency moves along the real axis; then, upon collision with eigenfrequencies of modes of opposite signature than that of the translation mode, it gives rise to a complex eigenfrequency quartet, signaling the presence of an oscillatory instability. The relevant eigenfrequencies can be determined by a quadratic characteristic equation which takes the form [64],

$$\lambda^2 + \frac{1}{4} M''(\tilde{x}_0) \left(1 - \frac{\lambda}{2}\right) = \mathcal{O}(\epsilon^2), \quad (23)$$

where eigenvalues λ are related to eigenfrequencies ω through $\lambda^2 = -\omega^2$. Since the roots of $M''(x_0)$ are the two fixed points $x_{0\pm}$, we may evaluate $M''(x_{0\pm})$ explicitly, and obtain:

$$M''(x_{0\pm}) = -2 \operatorname{sech}^2(x_{0\pm}) \tanh(x_{0\pm}) \times [A + B \tanh^2(x_{0\pm})]. \quad (24)$$

To this end, combining Eqs. (23) and (24) yields an analytical prediction for the magnitudes of the relevant eigenfrequencies, for the cases of solitons located at the hyperbolic or the elliptic fixed points of $W(x_0)$.

Figure 4 shows pertinent analytical results [depicted by (red) solid lines], which are compared with corresponding numerical results [depicted by (blue) points]. In particular, the top panel of the figure illustrates the dependence of the imaginary part of the eigenfrequency (real part of the eigenvalue) ω_i on the parameter $1 - B$ (with $B < 0$), for a soliton located at the hyperbolic fixed point, $x = x_{0+}$; this case is associated with the scenario $M''(x_0) < 0$. The middle and bottom panels of the figure shows the dependence of ω_i and ω_r on $1 - B$, but for a soliton located at the elliptic fixed point, $x = x_{0-}$; in this case, $M''(x_0) > 0$, corresponding to an oscillatory instability as mentioned above. It is readily observed that the agreement between the theoretical prediction of Eqs. (23) and (24) and the numerical result is very good; especially, for values of $1 - B$ close to unity, i.e., in the case $|B| \lesssim 0.15$ where perturbation theory is more accurate, the agreement is excellent.

We should also remark here that a similarly good agreement between analytical and numerical results was also found (results not shown here) upon using as an independent parameter the strength of the potential step ($\sim A$), instead of the strength of the nonlinearity step ($\sim B$), as in the case of Fig. 4.

III. DARK SOLITONS DYNAMICS

We now turn our attention to the dynamics of dark solitons near the potential and nonlinearity steps. We will use, as a guideline, the analytical results presented in the previous section, and particularly the form of the effective potential. Our aim is to study the scattering of a dark soliton, initially located in the region $x < L$ and moving to the right, at the potential and nonlinearity steps (similar considerations, for a soliton located in the region $x > L$ and moving to the left, are straightforward, hence only limited examples of the latter type will be presented). We will consider the scattering process in the presence of: (a) a single potential step, (b) a potential and nonlinearity step, and (c) two potential and nonlinearity steps.

Attention will be paid to possible trapping of the soliton in the vicinity of the location of the potential and nonlinearity steps, and particularly at the hyperbolic fixed point (when present) of the effective potential. Notice that in the context of optics such a soliton trapping effect could be viewed as a formation of surface dark solitons at the interfaces between optical media exhibiting different linear refractive indices and different defocusing Kerr nonlinearities (or atomic media bearing different linear potential and interparticle interaction properties at the two sides of the interface).

A. A single potential step

Our first scattering ‘‘experiment’’ refers to the case of a potential step only, corresponding to $A > 0$ and $B = 0$ (cf. inset I in Fig. 1). In this case, the effective potential has typically the form shown in the top panel of Fig. 5, while the associated phase-plane is shown in the middle panel of the same figure. Clearly, according to the particle picture for the soliton of the previous section, a dark soliton incident from the left towards the potential step can either be reflected or transmitted: if the soliton has a velocity $v = dx_0/dt$, and thus a kinetic energy

$$K = \frac{1}{2} v^2 = \frac{1}{2} \sin^2 \phi \approx \frac{1}{2} \phi^2, \quad (25)$$

smaller (greater) than the effective potential step $\Delta W = W(+\infty) - W(-\infty)$, as shown in the top panel of Fig. 5, then it will be reflected (transmitted). Notice the approximation ($\sin \phi \approx \phi$) here which is applicable for low speeds/kinetic energies. This consideration leads to $\phi < \phi_c$ or $\phi > \phi_c$ for reflection or transmission, where the critical value ϕ_c of the soliton phase angle is given by:

$$\phi_c = \sqrt{2\Delta W}. \quad (26)$$

In the numerical simulations, we found that the threshold between the two cases is quite sharp and is accurately predicted by Eq. (26). Indeed, consider the scenario shown in Fig. 5, corresponding to parameter values $V_L = 0$, $V_R = 0.01$, $\alpha_R = \alpha_L$ and $\mu_L = 1$. In this case, we find that $\Delta W = 4.99 \times 10^{-3}$, which leads to the critical value (for reflection/transmission) of the soliton phase angle $\phi_c = 9.99 \times 10^{-2}$. Then, for a soliton initially placed at

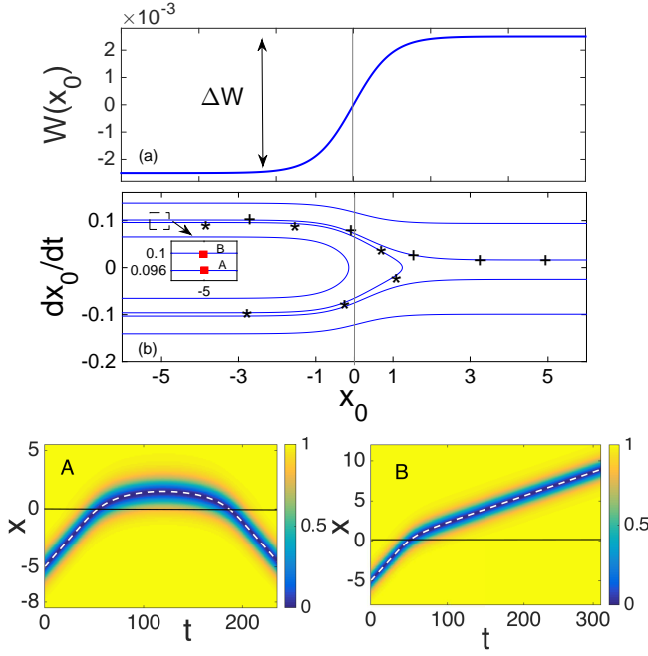


FIG. 5: (Color online) The case of a single potential step, $A = 0.01$ and $B = 0$, corresponding to $V_L = 0$, $V_R = 0.01$, $\alpha_R = \alpha_L$, and $\mu_L = 1$. Top panel (a): effective potential $W(x_0)$; shown also is the potential difference $\Delta W = W(+\infty) - W(-\infty) = 4.99 \times 10^{-3}$. Middle panel (b): corresponding phase plane; inset shows the initial conditions (red squares A and B) for the trajectories corresponding to reflection or transmission, while stars and crosses depict respective PDE results. Bottom panel: contour plots showing the evolution of the dark soliton density for the initial conditions depicted in the middle panel, i.e., $x_0 = -5$ and $\phi = 9.6 \times 10^{-2}$ (left), or $\phi = 0.1$ (right); note that, here, $\phi_c = 0.099$. Thick (blue) solid lines show PDE results, while dashed (white) lines depict ODE results.

$x_0 = -5$, and for initial velocities corresponding to phase angles $\phi = 9.6 \times 10^{-2}$ or $\phi = 0.1$, we observe reflection or transmission, respectively. The corresponding soliton trajectories are depicted both in the phase plane ($x_0, dx_0/dt$) in the middle panel of Fig. 5 and in the space-time contour plots showing the evolution of the soliton density in the bottom panels of the same figure (see trajectories A and B for reflection and transmission, respectively). Note that stars and crosses in the middle panel correspond to results obtained by direct numerical integration of the partial differential equation (PDE), Eq. (5), while the (white) dashed lines in the bottom panels depict results obtained by the ordinary differential equation (ODE), Eq. (14). Obviously, the agreement between theoretical predictions and numerical results is very good.

Here we should recall that in the case where the nonlinearity step is also present ($B \neq 0$), and when $B > -A$ (for $A > 0$) or $B < -A$ (for $A < 0$), the form of the effective potential is similar to the one shown in the top panel of Fig. 5. In such cases, corresponding results (not shown here) are qualitatively similar to the ones presented above (for $A \neq 0$ and $B = 0$); in addition, we have again captured accurately the velocity threshold for reflection/transmission.

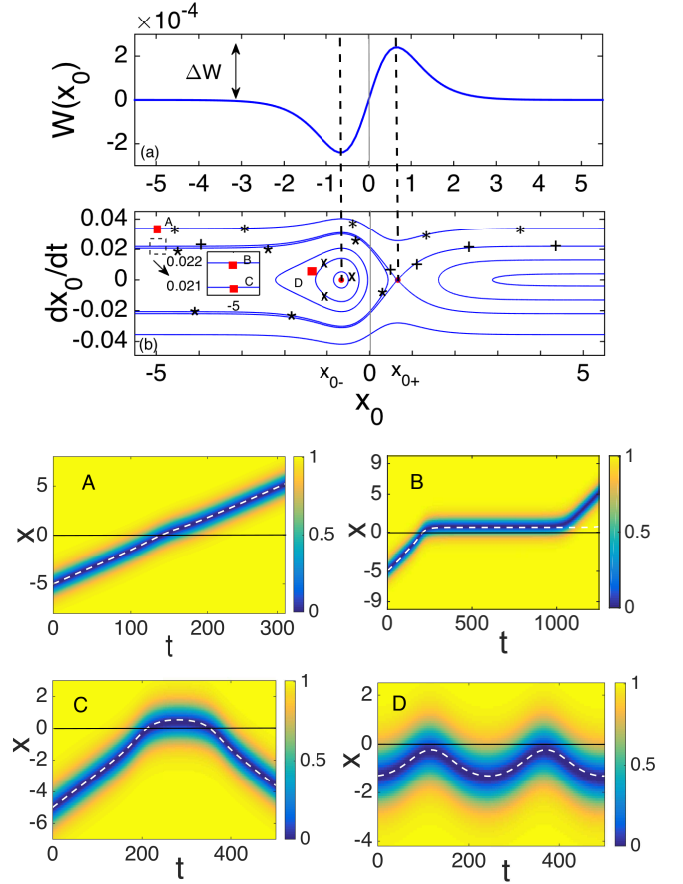


FIG. 6: (Color online) Similar to Fig. 5, but for a potential and a nonlinearity step, $A = 0.01$ and $B = -0.015$, corresponding to $V_L = 0$, $V_R = 0.01$, $\alpha_R/\alpha_L = 0.985$, and $\mu_L = 1$. Top and bottom panels show the effective potential $W(x_0)$ and the associated phase plane, respectively; the potential now features an elliptic and a hyperbolic fixed point at $x_0 \approx \pm 0.65$ (cf. vertical dashed lines). In the phase plane, initial conditions—marked with red squares—at points A ($x_0 = -5$, $\phi = 0.034$), B ($x_0 = -5$, $\phi = 0.022$), C ($x_0 = -5$, $\phi = 0.021$) and D ($x_0 = -1.3$, $\phi = 0.002$) lead to soliton transmission, quasi-trapping, reflection, and oscillations around the elliptic fixed point, respectively; asterisks, crosses and stars depict PDE results. The four bottom respective contour plots show the evolution of the soliton density; again, thick blue lines and white dashed lines depict PDE and ODE results, respectively.

B. A potential and a nonlinearity step

Next, we study the case where both a potential and a nonlinearity step are present (i.e., $A, B \neq 0$), and there exist fixed points of the effective potential. One such case that we consider in more detail below is the one corresponding to $A = 0.01$ and $B = -0.015$ (respective parameter values are $V_L = 0$, $V_R = 0.01$, $\alpha_R/\alpha_L = 0.985$, and $\mu_L = 1$). Note that for this choice the effective potential asymptotically vanishes, as shown in the top panel of Fig. 6; nevertheless, results qualitatively similar to the ones that we present below can also be obtained for nonvanishing asymptotics of $W(x_0)$.

The effective potential now features an elliptic and a hyper-

bolic fixed point, located at $x_0 \approx \mp 0.65$ respectively. In this case too, one can identify an energy threshold ΔW , now defined as $\Delta W = W(x_{0+}) - W(-\infty) = W(x_{0+})$, needed to be overcome by the soliton kinetic energy in order for the soliton to be transmitted (otherwise, i.e., for $K < \Delta W$, the soliton is reflected). Using the above parameter values, we find that $\Delta W = 2.4 \times 10^{-4}$ and, hence, according to Eq. (26), the critical phase angle for transmission/reflection is $\phi_c \approx 0.022$. In the simulations, we considered a soliton with initial position and phase angle $x_0 = -5$ and $\phi = 0.034 > \phi_c$, respectively (cf. point A in the phase plane shown in the second panel of Fig. 6), and found that, indeed, the soliton is transmitted through the effective potential barrier of strength ΔW . The respective trajectory (starting from point A) is shown in the second panel of Fig. 6. Stars along this trajectory, as well as contour plot A in the same figure, show PDE results obtained from direct numerical integration of Eq. (5); as in the case of Fig. 5, the (white) dashed line corresponds to the ODE result.

To study the possibility of soliton trapping, we have also used an initial condition at the stable branch, incoming towards the hyperbolic fixed point, namely $x_0 = -5$ and $\phi = \phi_c \approx 0.022$ (point B in the second panel of Fig. 6). In this case, the soliton reaches at the location of the hyperbolic fixed point (cf. incoming branch, marked with pluses) and appears to be trapped at the saddle; however, this trapping occurs only for a finite time (for $t \approx 600$). At the PDE level, this can be understood by the fact that such a configuration (i.e., a stationary dark soliton located at the hyperbolic fixed point) is unstable, as per the analysis of Sec. II.D. Then, the soliton escapes and moves to the region of $x > 0$, following the trajectory marked with pluses for $x > x_{0+}$ (here, the pluses depict the PDE results). The corresponding contour plot B, in the third panel of Fig. 6, shows the evolution of the dark soliton density. Note that, in this case, the result obtained by the ODE (cf. white dashed line) is only accurate up to the escape time, as small perturbations within the infinite-dimensional system destroy the delicate balance of the unstable fixed point.

For the same form of the effective potential, we have also used initial conditions that lead to soliton reflection. In particular, we have again used $x_0 = -5$ and $\phi = 0.021 < \phi_c$, as well as an initial soliton location closer to the potential and nonlinearity step, namely $x_0 = -1.3$, and $\phi = 0.002$. These initial conditions are respectively indicated by the (red) squares C and D in the second panel of Fig. 6. Relevant trajectories in the phase plane, as well as respective PDE results (cf. stars and X marks), can also be found in the same panel, while contour plots C and D in the bottom panel of Fig. 6 show the evolution of the soliton densities. It can readily be observed that for the slightly subcritical value of the phase angle ($\phi = 0.021$), the soliton is again quasi-trapped at the hyperbolic fixed point, but for a significantly smaller time (for $t \approx 150$). On the other hand, when the soliton is initially located closer to the steps and has a sufficiently small initial velocity, it performs oscillations, following the periodic orbit shown in the second panel of Fig. 6.

In all the above cases, we find a very good agreement between the analytical predictions and the numerical results. Similar agreement was also found for other forms of the ef-

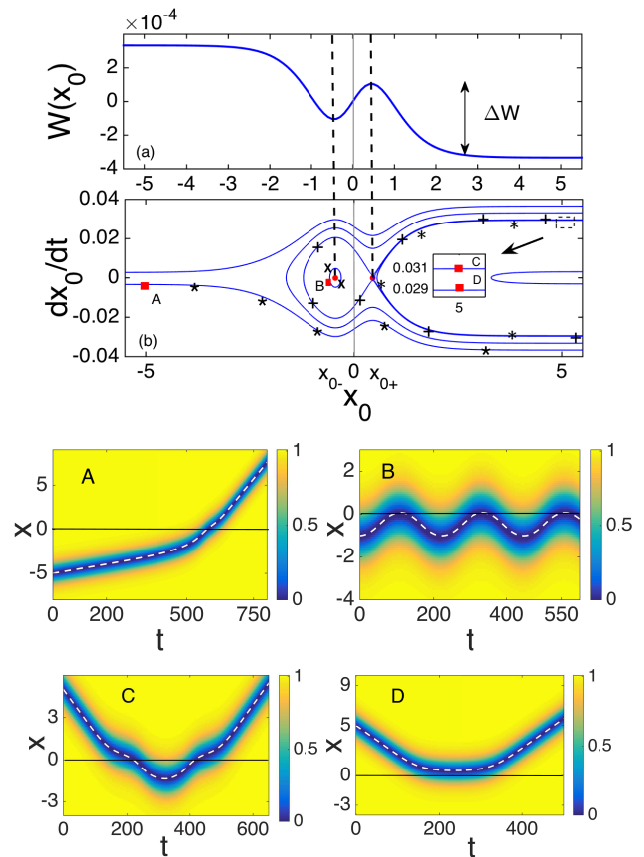


FIG. 7: (Color online) Similar to Fig. 6, for a potential and a nonlinearity step, but now for $A = 0.01$ and $B = -0.017$, corresponding to $V_L = 0$, $V_R = 0.01$, $\alpha_R/\alpha_L = 0.983$, and $\mu_L = 1$. The effective potential $W(x_0)$ (top panel), exhibits an elliptic and a hyperbolic fixed point, at $x_{0\pm} = \pm 0.44$ (vertical dashed lines). In the associated phase plane (second panel) shown are initial conditions, for a soliton moving to the right, at points A ($x_0 = -5$, $\phi = 0.005$) and B ($x_0 = -1$, $\phi = 0.001$), as well as for a soliton moving to the left, at points C ($x_0 = 5$, $\phi = 0.031 > \phi_c \approx 0.030$) and D ($x_0 = 5$, $\phi = 0.029 < \phi_c$); in the relevant trajectories, stars, X marks, pluses and asterisks, respectively, denote PDE results. Corresponding contour plots for the soliton density are shown in the bottom panels, with the dashed white lines depicting ODE results.

fective potential, as shown, e.g., in the example of Fig. 7 (see also inset III of Fig. 1). For this form of $W(x_0)$, parameters A and B are $A = 0.01$ and $B = -0.017$ (for $V_L = 0$, $V_R = 0.01$, $\alpha_R/\alpha_L = 0.983$, and $\mu_L = 1$), while there exist again an elliptic and a hyperbolic fixed point, at $x_{0\pm} = \pm 0.44$ respectively. In such a situation, if a soliton moves from the left towards the potential and nonlinearity steps, and is placed sufficiently far from (close to) them – cf. initial condition at point A (point B) – then it will be transmitted (perform oscillations around x_{0-}). On the other hand, if a soliton is initially placed at some $x_0 > x_{0+}$ and moves to the left towards the potential and nonlinearity steps, it faces an effective barrier ΔW (cf. top panel of Fig. 7), now defined as $\Delta W = W(x_{0+}) - W(+\infty)$. In this case too, choosing an initial condition corresponding to the stable branch, incoming

towards x_{0+} , i.e., for the critical phase angle $\phi_c \approx 0.03$, it is possible and achieve quasi-trapping of the soliton for a finite time, of the order of $t \approx 600$. As such a situation was already discussed above (cf. panel B of Fig. 6), here we present results pertaining to the slightly supercritical and subcritical cases, namely $\phi = 0.031 > \phi_c$ and $\phi = 0.029 < \phi_c$; cf. (red) squares C and D in the second panel, and corresponding contour plots in the bottom panel of Fig. 7. It is readily observed that, in the former case, the soliton is initially transmitted through the interface; however, it then follows a trajectory surrounding the homoclinic orbit (see the orbit marked with plus symbols, which depicts the PDE results, in the second panel of Fig. 7), and is eventually reflected. In the case $\phi = 0.029 < \phi_c$, the soliton reaches x_{0+} , stays there for a time $t \approx 180$, and eventually is reflected back following the trajectory marked with asterisks (see second panel of Fig. 7). In all cases pertaining to this form of $W(x_0)$, the agreement between the analytical predictions and the numerical results is very good as well.

C. Rectangular barriers

Our analytical approximation can straightforwardly be extended to the case of multiple potential and nonlinearity steps. Here, we will present results for such a case, where two steps, located at $x = -L$ and $x = L$, are combined so as to form rectangular barriers, in both the linear potential and the nonlinearity of the system. In particular, we consider the following profiles for the potential and the scattering length:

$$V(x) = V_b(x) + \begin{cases} V_R, & |x| > L \\ V_L, & |x| < L \end{cases}, \quad (27)$$

$$\alpha(x) = \begin{cases} \alpha_R, & |x| > L \\ \alpha_L, & |x| < L \end{cases}. \quad (28)$$

In such a situation, the effective potential can be found following the lines of the analysis presented in Sec. II.B: taking into regard that the perturbation $P(v)$ in Eq. (7) has now the form:

$$P(v) = (A + B|v|^2)v[\mathcal{H}(x + L) - \mathcal{H}(x - L)], \quad (29)$$

it is straightforward to find that the relevant effective potential is given by:

$$W(x_0) = \frac{1}{8}(2A + B)[\tanh(L - x_0) + \tanh(L + x_0)] + \frac{1}{24}B[\tanh^3(L - x_0) + \tanh^3(L + x_0)]. \quad (30)$$

Typically, i.e., for sufficiently large arbitrary values of L , the effective potential is as shown in the top panel of Fig. 8; in this example, we used $L = 5$, while $A = 0.01$ and $B = -0.015$. It is readily observed that, in this case, associated with such a potential and a nonlinearity barrier, is an effective potential of the form of a superposition of the ones shown in Fig. 6, which are now located at ± 5 . The associated

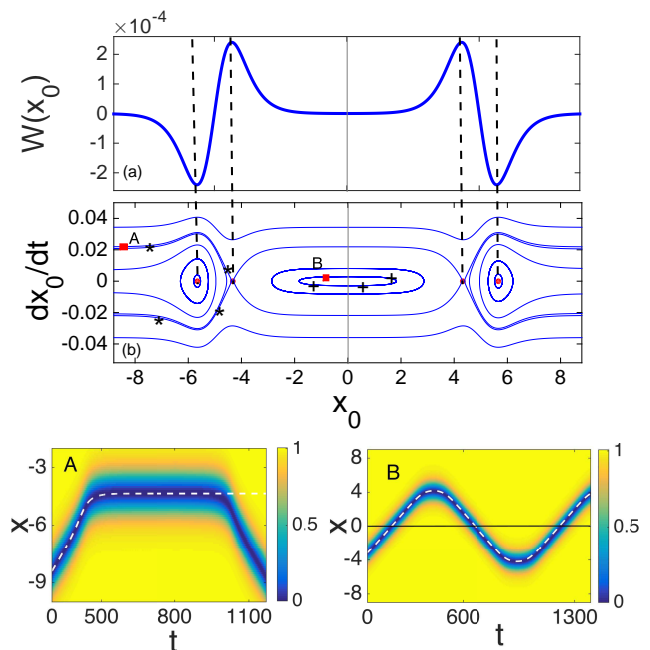


FIG. 8: (Color online) The case of two potential and nonlinearity steps forming respective rectangular barriers, for $L = 5$, $A = 0.01$ and $B = -0.015$, corresponding to $V_L = 0$, $V_R = 0.01$, $\alpha_R/\alpha_L = 0.985$, $\mu_L = 1$. Top panel (a): the effective potential $W(x_0)$ [cf. Eq. (30)], featuring elliptic fixed points at the origin and at ± 5.66 , and a pair of hyperbolic fixed points at ± 4.34 . Middle panel (b): the associated phase plane; (red) squares A and B depict different initial conditions, corresponding to quasi-trapping or oscillations, while stars and crosses depict respective PDE results. Bottom panels: contour plots showing the evolution of the dark soliton density for the initial conditions depicted in the middle panel, i.e., $x_0 = -8.6$ and $\phi = 2.2 \times 10^{-2}$ (left), or $x_0 = -3$ and $\phi = 3 \times 10^{-3}$ (right); here, as before, dashed (white) lines depict ODE results.

phase plane is shown in the middle panel of Fig. 8; shown also are initial conditions corresponding to soliton quasi-trapping, or oscillations around the elliptic fixed point at the origin – cf. red square points A and B, respectively. The corresponding soliton trajectories are depicted both in the phase plane in the middle panel of Fig. 8 and in the space-time contour plots showing the evolution of the soliton density in the bottom panels of the same figure. Note that stars and plus symbols in the middle panel correspond to PDE results, obtained in the framework of Eq. (5), while the (white) dashed lines in the bottom panels depict ODE results, obtained by Eq. (14) for the potential in Eq. (30). Obviously, once again, agreement between theoretical predictions and numerical results is very good.

An interesting situation occurs as L decreases. To better illustrate what happens in this case, and also to make connections with earlier work [9], we consider the simpler case of $B = 0$ (i.e., the nonlinearity step is absent). Then, assuming that $A = b/(2L)$ (with b being an arbitrary small parameter), and in the limit of $L \rightarrow 0$, the potential step takes the form of a delta-like impurity of strength b . In this case, the effective potential of Eq. (30) is reduced to the form

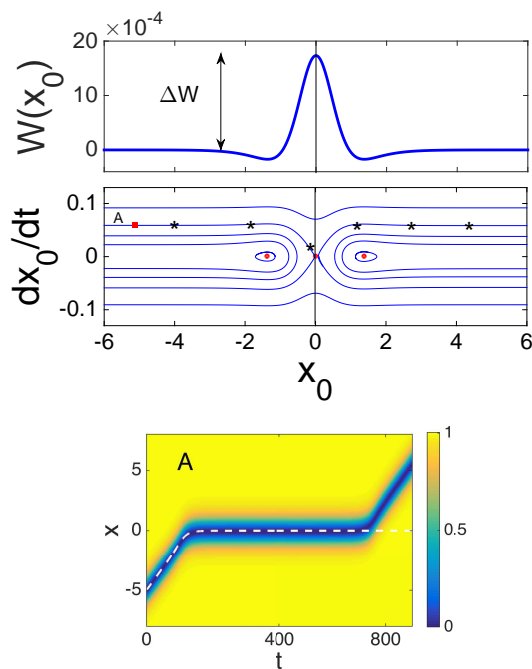


FIG. 9: (Color online) The case of two potential and nonlinearity steps forming respective rectangular barriers, for $L = 0.1$, $A = 0.1$ and $B = -0.13$, corresponding to $a_R/a_L = 0.87$, $V_R = 0.1$ and $\mu_L = 1$. Top panel: the effective potential $W(x_0)$, featuring a hyperbolic fixed point at the origin and a pair of elliptic fixed points at ± 1.38 . Middle panel: the associated phase plane; (red) square A depicts an initial condition corresponding to quasi-trapping of the soliton, while stars depict respective PDE results. Bottom panel: contour plot showing the evolution of the dark soliton density for the initial condition depicted in the middle panel, i.e., $x_0 = -5$ and $\phi = 5.8 \times 10^{-2}$; as before, dashed (white) lines depict ODE results.

$W(x_0) = (b/4)\text{sech}^2(x_0)$. This result recovers the one reported in Ref. [9] (see also Refs. [8, 10]), where the interaction of dark solitons with localized impurities was studied; cf. Eq. (16) of that work, but in the absence of the trapping potential U_{tr} .

In the same limiting case of small L , and for $B \neq 0$, the effective potential has typically the form shown in the top panel of Fig. 9; here, we use $L = 0.1$, while $A = 0.1$ and $B = -0.13$, corresponding to $a_R/a_L = 0.87$, $V_R = 0.1$ and $\mu_L = 1$. Comparing this form of $W(x_0)$ with the one shown in Fig. 8, it becomes clear that as $L \rightarrow 0$, the individual parts of the effective potential of Fig. 8 pertaining to the two potential/nonlinearity steps move towards the origin. There, they merge at the location of the “central” elliptic fixed point, which becomes unstable through a pitchfork bifurcation. As a result of this process, an unstable (hyperbolic) fixed point emerges at the origin, while the “outer” pair of the elliptic fixed points (cf. Fig. 8) also drift towards the origin – in this case, they are located at ± 1.38 .

In the middle panel of Fig. 9, shown also is the phase plane associated to the effective potential of the top panel. As in the cases studied in the previous sections, we may investigate possible quasi-trapping of the soliton, using an initial

condition at the stable branch, incoming towards the hyperbolic fixed point at the origin. Indeed, choosing $x_0 = -5$ and $\phi = \phi_c = 5.8 \times 10^{-2}$ (notice that here, the corresponding effective barrier $\Delta W = 1.7 \times 10^{-3}$ – cf. top panel of Fig. 9), we find the following: the soliton arrives at the origin, stays there for a time $t \approx 600$, and then it is transmitted through the region $x > 0$. In fact, the corresponding trajectory found at the PDE level is depicted by stars in the middle panel of Fig. 9, while the relevant contour plot showing the evolution of the soliton density is shown in the bottom panel of the same figure. Notice, again, the fairly good agreement between numerical and analytical results.

We note that for the same parameter values, but for $B = 0$, elliptic fixed points do not exist, and the effective potential has simply the form of a sech^2 barrier, as mentioned above (see also work of Ref. [9]). In this case, starting from the same initial position, $x_0 = -5$, and for $\phi = 0.1$ (corresponding to $\phi_c = \sqrt{2\Delta W} \approx 0.1$), we find that the trapping time is $t \approx 320$, i.e., almost half of the one that was when the nonlinearity steps/barriers are present (results not shown here). This observation, along with the results presented in the previous sections, indicate that nonlinearity steps/barriers are necessary either to facilitate or enhance soliton trapping in such inhomogeneous settings.

IV. DISCUSSION AND CONCLUSIONS

We have studied matter-wave dark solitons near linear potential and nonlinearity steps, superimposed on a box-like potential that was assumed to confine the atomic Bose-Einstein condensate. The formulation of the problem finds a direct application in the context of nonlinear optics: the pertinent model can be used to describe the evolution of beams, carrying dark solitons, near interfaces separating optical media with different linear refractive indices and different defocusing Kerr nonlinearities.

Assuming that the potential/nonlinearity steps were small, we employed perturbation theory for dark solitons to show that, in the adiabatic approximation, solitons behave as equivalent particles moving in the presence of an effective potential. The latter was found to exhibit various forms, ranging from simple tanh-shaped steps – for a spatially homogeneous scattering length (or same Kerr nonlinearity, in the context of optics) – to more complex forms, featuring hyperbolic and elliptic fixed points – in the presence of steps in the scattering length (different Kerr nonlinearities).

In the latter case, we found that stationary soliton states do exist at the fixed points of the effective potential. Using a Bogoliubov-de Gennes (BdG) analysis, we showed that these states are unstable: dark solitons at the hyperbolic fixed points have a pair of unstable real eigenvalues, while those at the elliptic fixed points have a complex eigenfrequency quartet, dictating a purely exponential or an oscillatory instability, respectively. We also used an analytical approximation to determine the real and imaginary parts of the relevant eigenfrequencies as functions of the nonlinearity step strength. The analytical predictions were found to be in good agreement with corre-

sponding numerical findings obtained in the framework of the BdG analysis.

We then studied systematically soliton dynamics, for a variety of parameter values corresponding to all possible forms of the effective potential. Adopting the aforementioned equivalent particle picture, we found analytically necessary conditions for soliton reflection at, or transmission through the potential and nonlinearity steps: these correspond to initial soliton velocities smaller or greater to the energy of the effective steps/barriers predicted by the perturbation theory and the equivalent particle picture.

We also investigated the possibility of soliton (quasi-) trapping, for initial conditions corresponding to the incoming, stable manifolds of the hyperbolic fixed points (which exist only for inhomogeneous nonlinearities). In the context of optics, such a trapping can be regarded as the formation of surface dark solitons at the interface between dielectrics of different refractive indices. We found that trapping is possible, but only for a finite time. This effect can be understood by the fact that stationary solitons at the hyperbolic fixed points are unstable, as was corroborated by the BdG analysis. Thus small perturbations (at the PDE level) eventually cause the departure of the solitary wave from the relevant fixed points. Nevertheless, it should be pointed out that the time of soliton quasi-trapping was found to be of the order of $600\sqrt{2}\xi/c_S$ in physical units; thus, typically, for a healing length ξ of the order of a micron and a speed of sound c_s of the order of a millimeter-per-second, trapping time may be of the order of ≈ 850 ms. This indicates that such a soliton quasi-trapping effect may be observed in real experiments. Note that in all scenarios (reflection, transmission, quasi-trapping) our analytical predictions were found to be in very good agreement with direct numerical simulations in the framework of the original Gross-Pitaevskii model.

We have also extended our considerations to study cases involving two potential and nonlinearity steps, that are combined so as to form corresponding rectangular barriers. Reflection, transmission and quasi-trapping of solitons in such cases were studied too, again with a very good agreement between analytical and numerical results. In this setting, special attention was paid to the limiting case of infinitesimally small distance between the adjacent potential/nonlinearity steps that form the barriers. In this case, we found that, due to a pitchfork bifurcation, the stability of the fixed point of the effective potential at the barrier center changes: out of two hyperbolic and one elliptic fixed point, a hyperbolic fixed point emerges, and the potential rectangular barrier is reduced to a delta-like

impurity. The latter is described by a sech^2 effective potential, in accordance with the analysis of earlier works [8–10].

Our methodology and results pose a number of interesting questions for future studies. First, it would be interesting to investigate how our perturbative results change as the potential/nonlinearity steps or barriers become larger, and/or attain more realistic shapes (including steps bearing finite widths, as well as Gaussian barriers – cf., e.g., recent work of Ref. [13]). In the same context, a systematic numerical – and, possibly, also analytical – study of the radiation of solitons during reflection or transmission (along the lines, e.g., of Ref. [54]) should also provide a more complete picture in this problem. Furthermore, a systematic study of settings involving multiple such steps/barriers, and an investigation of the possibility of soliton trapping therein, would be particularly relevant. In such settings, investigation of the dynamics of moving steps/barriers could find direct applications to fundamental studies relevant, e.g., to superfluidity (see, for instance, Ref. [19]), transport of BECs [20], and even Hawking radiation in analog black hole lasers implemented with BECs [66]. Finally, extension of our analysis to higher-dimensional settings, would also be particularly challenging: first, in order to investigate transverse excitation effects that are not captured within the quasi-1D setting, and second to study similar problems with vortices and other vortex structures. See, e.g., Ref. [67] for a summary of relevant studies in higher-dimensional settings, and Ref. [68] for a recent example of manipulation/control of vortex patterns and their formation via Gaussian barriers, motivated by experimentally accessible laser beams.

Acknowledgments

The work of F.T. and D.J.F. was partially supported by the Special Account for Research Grants of the University of Athens. The work of F.T. and Z.A.A. was partially supported by Qatar University under the scope of the Internal Grant QUUG-CAS-DMSP-13/14-7. F.T. acknowledges hospitality at Qatar University, where most of this work was carried out. The work of P.G.K. at Los Alamos is partially supported by the US Department of Energy. P.G.K. also gratefully acknowledges the support of NSF-DMS-1312856, BSF-2010239, as well as from the US-AFOSR under grant FA9550-12-1-0332, and the ERC under FP7, Marie Curie Actions, People, International Research Staff Exchange Scheme (IRSES-605096).

[1] Yu. S. Kivshar and B. A. Malomed, *Rev. Mod. Phys.* **61**, 763 (1989).
 [2] I. M. Lifshitz and A. M. Kosevich, *Rep. Prog. Phys.* **29**, 217 (1966).
 [3] I. Ianni, S. L. Coz, and J. Royer, arXiv:1506.03761.
 [4] A. M. Kosevich, *Physica D* **41**, 253 (1990).
 [5] X. D. Cao and B. A. Malomed, *Phys. Lett. A* **206**, 177 (1995).
 [6] R. H. Goodman, P. J. Holmes, and M. I. Weinstein, *Physica D*

192, 215 (2004).
 [7] J. Holmer, J. Marzuola, and M. Zworski, *Comm. Math. Phys.* **274**, 187 (2007); J. Holmer, J. Marzuola, and M. Zworski, *J. Nonlin. Sci.* **17**, 349 (2007).
 [8] V. V. Konotop, V. M. Pérez-García, Y.-F. Tang, and L. Vázquez, *Phys. Lett. A* **236**, 314 (1997).
 [9] D. J. Frantzeskakis, G. Theocharis, F. K. Diakonov, P. Schmelcher, and Yu. S. Kivshar, *Phys. Rev. A* **66**, 053608

- (2002).
- [10] N. Bilas and N. Pavloff, Phys. Rev. A **72**, 033618 (2005).
- [11] N. Bilas and N. Pavloff, Phys. Rev. Lett. **95**, 130403 (2005).
- [12] G. Herring, P. G. Kevrekidis, R. Carretero-González, B. A. Malomed, D. J. Frantzeskakis, and A. R. Bishop, Phys. Lett. A **345**, 144 (2005).
- [13] I. Hans, J. Stockhofe, and P. Schmelcher, Phys. Rev. A **92**, 013627 (2015).
- [14] T. Ernst and J. Brand, Phys. Rev. A **81**, 033614 (2010).
- [15] C. Lee and J. Brand, Europhys. Lett. **73**, 321 (2006).
- [16] J. L. Helm, T. P. Billam, and S. A. Gardiner, Phys. Rev. A **85**, 053621 (2012).
- [17] A. D. Martin and J. Ruostekoski, New J. Phys. **14**, 043040 (2012).
- [18] Y. Nogami and F. M. Toyama, Phys. Lett. A **184**, 245-250 (1994).
- [19] P. Engels and C. Atherton, Phys. Rev. Lett. **99**, 160405 (2007).
- [20] D. Dries, S. E. Pollack, J. M. Hitchcock, and R. G. Hulet, Phys. Rev. A **82**, 033603 (2010).
- [21] J. Cuevas, P. G. Kevrekidis, B. A. Malomed, P. Dyke, and R. G. Hulet, New J. Phys. **15**, 063006 (2013).
- [22] A. L. Marchant, T. P. Billam, T. P. Wiles, M. M. H. Yu, S. A. Gardiner, and S. L. Cornish, Nat. Com. **4**, 1865 (2013).
- [23] V. Achilleos, P. G. Kevrekidis, V. M. Rothos, and D. J. Frantzeskakis, Phys. Rev. A **84**, 053626 (2011).
- [24] A. Álvarez, J. Cuevas, F. R. Romero, C. Hamner, J. J. Chang, P. Engels, P. G. Kevrekidis, and D. J. Frantzeskakis, J. Phys. B: At. Mol. Opt. Phys. **46**, 065302 (2013).
- [25] G. Theocharis, P. Schmelcher, P. G. Kevrekidis, and D. J. Frantzeskakis, Phys. Rev. A **72**, 033614 (2005).
- [26] S. Middelkamp, P. G. Kevrekidis, D. J. Frantzeskakis and P. Schmelcher, Phys. Lett. A **373**, 262268 (2009).
- [27] Y. V. Kartashov, B. A. Malomed, and L. Torner, Rev. Mod. Phys. **83**, 247 (2011).
- [28] F. Kh. Abdullaev and M. Salerno, J. Phys. B: At. Mol. Opt. Phys. **36**, 2851 (2003).
- [29] M. I. Rodas-Verde, H. Michinel, and V. M. Pérez-García, Phys. Rev. Lett. **95**, 153903 (2005); A. V. Carpentier, H. Michinel, M. I. Rodas-Verde, and V. M. Pérez-García, Phys. Rev. A **74**, 013619 (2006).
- [30] F. Tsitoura, P. Krüger, P. G. Kevrekidis, and D. J. Frantzeskakis, Phys. Rev. A, **91**, 033633 (2015).
- [31] G. Theocharis, P. Schmelcher, P. G. Kevrekidis, and D. J. Frantzeskakis, Phys. Rev. A **74**, 053614 (2006); J. Garnier and F. Kh. Abdullaev, *ibid.* **74**, 013604 (2006); P. Niarchou, G. Theocharis, P. G. Kevrekidis, P. Schmelcher, and D. J. Frantzeskakis, *ibid.* **76**, 023615 (2007).
- [32] C. Wang, K.J.H. Law, P. G. Kevrekidis, and M. A. Porter, Phys. Rev. A **87**, 023621 (2013).
- [33] G. Dong, B. Hu, and W. Lu, Phys. Rev. A **74**, 063601 (2006).
- [34] H. Sakaguchi and B. A. Malomed, Phys. Rev. A **81**, 013624 (2010);
- [35] S. Holmes, M. A. Porter, P. Krüger, and P. G. Kevrekidis, Phys. Rev. A **88**, 033627 (2013).
- [36] K. Hizanidis, Y. Kominis, and N. K. Efremidis, Opt. Express **16**, 18296 (2008).
- [37] R. Marangell, C.K.R.T. Jones, and H. Susanto, Nonlinearity **23**, 2059 (2010).
- [38] R. Marangell, H. Susanto, and C.K.R.T. Jones, J. Diff. Eq. **253**, 1191 (2012).
- [39] C. Wang, P. G. Kevrekidis, T. P. Horikis, and D. J. Frantzeskakis, Phys. Lett. A **374**, 3863 (2010); T. Mithun, K. Porsezian, and B. Dey, Phys. Rev. E **88**, 012904 (2013).
- [40] F. Pinsker, N. G. Berloff, and V. M. Pérez-García, Phys. Rev. A **87**, 053624 (2013).
- [41] A. Balaz, R. Paun, A. I. Nicolin, S. Balasubramanian, and R. Ramaswamy, Phys. Rev. A **89**, 023609 (2014).
- [42] T. Kaneda and H. Saito, Phys. Rev. A **90**, 053632 (2014).
- [43] A. Weller, J. P. Ronzheimer, C. Gross, J. Esteve, M. K. Oberthaler, D. J. Frantzeskakis, G. Theocharis, and P. G. Kevrekidis, Phys. Rev. Lett. **101**, 130401 (2008); S. Stellmer, P. Soltan-Panahi, S. Dörscher, M. Baumert, E.-M. Richter, J. Kronjäger, K. Bongs, and K. Sengstock, Nat. Phys. **4**, 496 (2008); S. Stellmer, C. Becker, P. Soltan-Panahi, E.-M. Richter, S. Dörscher, M. Baumert, J. Kronjäger, K. Bongs, and K. Sengstock, Phys. Rev. Lett. **101**, 120406 (2008); G. Theocharis, A. Weller, J. P. Ronzheimer, C. Gross, M. K. Oberthaler, P. G. Kevrekidis, and D. J. Frantzeskakis, Phys. Rev. A **81**, 063604 (2010).
- [44] B. T. Seaman, L. D. Carr, and M. J. Holland, Phys. Rev. A, **71**, 033609 (2005).
- [45] L. D. Carr, R. R. Miller, D. R. Bolton, and S. A. Strong, Phys. Rev. A **86**, 023621 (2012).
- [46] S. Inouye, M. R. Andrews, J. Stenger, H. J. Miesner, D. M. Stamper-Kurn, and W. Ketterle, Nature (London) **392**, 151 (1998); J. Stenger, S. Inouye, M. R. Andrews, H.-J. Miesner, D. M. Stamper-Kurn, and W. Ketterle, Phys. Rev. Lett. **82**, 2422 (1999); J. L. Roberts, N. R. Claussen, J. P. Burke, Jr., C. H. Greene, E. A. Cornell, and C. E. Wieman, *ibid.* **81**, 5109 (1998); S. L. Cornish, N. R. Claussen, J. L. Roberts, E. A. Cornell, and C. E. Wieman, *ibid.* **85**, 1795 (2000).
- [47] F. K. Fatemi, K. M. Jones, and P. D. Lett, Phys. Rev. Lett. **85**, 4462 (2000); M. Theis, G. Thalhammer, K. Winkler, M. Hellwig, G. Ruff, R. Grimm, and J. H. Denschlag, *ibid.* **93**, 123001 (2004).
- [48] A. C. Newell and J. V. Moloney, *Nonlinear Optics* (Addison-Wesley, Redwood City, CA, 1992).
- [49] A. B. Aceves, J. V. Moloney, and A. C. Newell, J. Opt. Soc. Am. B **5**, 559 (1988); Phys. Lett. A **129**, 231 (1988); Phys. Rev. A **39**, 1809 (1989); *ibid.* **39**, 1828 (1989).
- [50] Yu. S. Kivshar, A. M. Kosevich, and O. A. Chubykalo, Phys. Rev. A **41**, 1677 (1990).
- [51] Yu. S. Kivshar and M. L. Quiroga-Teixeiro, Phys. Rev. A **48**, 4750 (1993).
- [52] Y. Kominis and K. Hizanidis, Phys. Rev. Lett. **102**, 133903 (2009).
- [53] H. Sakaguchi and M. Tamura, J. Phys. Soc. Jpn. **74**, 292 (2005).
- [54] N. G. Parker, N. P. Proukakis, M. Leadbeater, and C. S. Adams, J. Phys. B: At. Mol. Opt. Phys. **36** 2891 (2003).
- [55] N. P. Proukakis, N. G. Parker, D. J. Frantzeskakis, and C. S. Adams, J. Opt. B: Quantum Semiclass. Opt. **6**, S380 (2004).
- [56] H. Sakaguchi, Laser Phys. **16**, 340 (2006).
- [57] L. P. Pitaevskii and S. Stringari, *Bose-Einstein Condensation* (Oxford University Press, Oxford, 2003).
- [58] P. G. Kevrekidis, D. J. Frantzeskakis, and R. Carretero-González (eds.), *Emergent Nonlinear Phenomena in Bose-Einstein Condensates: Theory and Experiment* (Springer-Verlag, Berlin, 2008); R. Carretero-González, D. J. Frantzeskakis, and P. G. Kevrekidis, Nonlinearity **21**, 139 (2008).
- [59] R. Folman, P. Krüger, J. Denschlag, J. Schmiedmayer, and C. Henkel, Adv. At. Mol. Opt. Phys. **48**, 263 (2002).
- [60] L. D. Carr, C. W. Clark, and W. P. Reinhardt, Phys. Rev. A **62**, 063610 (2000).
- [61] Yu. S. Kivshar and X. Yang, Phys. Rev. E **49**, 1657 (1994).
- [62] D. J. Frantzeskakis, J. Phys. A: Math. Theor. **43**, 213001 (2010).
- [63] M. J. Ablowitz, S. D. Nixon, T. P. Horikis, and D. J. Frantzeskakis, Proc. R. Soc. A **2133**, 2597 (2011).

- [64] D. E. Pelinovsky and P. G. Kevrekidis, *ZAMP* **59**, 559 (2008).
- [65] A. S. Rodrigues, P. G. Kevrekidis, Mason A. Porter, D. J. Frantzeskakis, P. Schmelcher, and A. R. Bishop, *Phys. Rev. A* **78**, 013611 (2008).
- [66] J. Steinhauer, *Nat. Phys.* **10**, 864 (2014).
- [67] P. G. Kevrekidis, D. J. Frantzeskakis, and R. Carretero-González, *The defocusing Nonlinear Schrödinger Equation: From Dark Solitons to Vortices and Vortex Rings* (SIAM, Philadelphia, 2015).
- [68] B. Gertjerenken, P. G. Kevrekidis, R. Carretero-González, and B. P. Anderson, arXiv:1508.07152.